Available online at www.sciencedirect.com
ScienceDirect
Ceramics International 34 (2008) 51–56
CERAMICS INTERNATIONAL
www.elsevier.com/locate/ceramint

Investigation on the microstructure of self-reinforced Nd-α-sialon ceramics

Chunfeng Liu *, Feng Ye, Yu Zhou, Qingchang Meng

Institute for Advanced Ceramics, Harbin Institute of Technology, Harbin 150001, PR China

Received 25 January 2006; received in revised form 22 February 2006; accepted 21 August 2006

Abstract

α-Sialon ceramics doped with Nd_2O_3 were prepared by hot-pressing sintering at 1900 °C holding for 1 h with a heat preservation for 1 h at 1500 °C. Microscopic observations indicate that elongated α-sialon grains appear and are embedded in the fine equiaxed-grain matrix. A small amount of β-sialon phases and secondary crystallized phases M′ ($Nd_2Si_{3-x}Al_xO_{3+x}N_{4-x}$) also exist in the Nd-α-sialon ceramic. A core/shell structure can be found in the elongated α-sialon and β-sialon grains with a high aspect ratio, in which some misfit dislocations surround the core. The 21R AlN-polytype was observed by transmission electron microscopy (TEM), which could not be detected by X-ray diffraction (XRD) due to its trace amount. Different nucleation and growth modes of sialon grains were also discussed.

Keywords: α-Sialon; Ceramics; Nd_2O_3; Microstructure

1. Introduction

The α-sialon ceramics have been attracting attention for their several potential engineering applications because of their superior combination of properties, such as, high hardness, good thermal and chemical stability and excellent resistance to frication and wear [1,2]. In particular, the development of self-reinforced α-sialon ceramics with whisker-like microstructure further increases interest in these ceramics [3]. In order to obtain elongated α-sialon microstructure, Shen et al. [4,5] prepared α-sialon ceramics by spark plasma sintering (SPS), and Chen and Rosenflanz [3] used β-Si_3N_4 as starting power instead of α-Si_3N_4. Several metal cations, i.e. Li^+, Ca^{2+}, Mg^{2+}, and some rare earth cations have been used to stabilize α-sialon so as to obtain elongated grains and thus increase the fracture toughness of these α-sialon ceramics [6–11].

Nd_2O_3, as a rare earth additive, was also used to stabilize α-sialon ceramics. Owing to the relatively larger size of Nd cation, it is ready to obtain elongated α-sialon grains with higher aspect ratio, and hence increasing the toughness of the α-sialons [3,12,13]. Some researches indicate that it is difficult to obtain pure Nd-α-sialon, and there commonly exist a small amount of β-sialon, melilite (M′) and 21R AlN-polytypoid, which results a slight decreased hardness comparing with that doped with other small size cations [12,13]. The investigation on phase relationship and phase regions in Nd–Si–Al–O–N system indicates that the α-sialon region is smaller for larger rare-earth cation (Nd) and the β-sialon–α-sialon phase lines shift toward the NdN:3AlN line in the case of Nd cation [14]. The stability of α-sialon decreases at lower temperatures and especially with larger cations, and α-sialon region becomes larger with the increase of temperature [14]. Huang and Chen [15] and Sun et al. [16,17] did some research on rare-earth melilite solid solution and its phase relations with neighboring phases and nitrogen-rich liquid phase region in the Nd–Si–Al–O–N system, respectively. And some compatibility tetrahedra have been established in this region. Besides, the thermal stability and oxidation properties of the Nd-α-sialon ceramics have also been intensively estimated [14,18–21].

Due to the great dependence of the properties on microstructure, many studies on microstructure development of α-sialon ceramics have been widely investigated, especially on nucleation and growth of α-sialon grain [6,7,22,23]. However, the reports on the microstructure of Nd-α-sialon ceramics are scarce. In this work, therefore, more attention was

---

* Corresponding author at: P.O. Box 433, School of Materials Science and Engineering, Harbin Institute of Technology, Harbin 150001, PR China. Tel.: +86 451 86402040x8520; fax: +86 451 86414291.

0272-8842/$32.00
doi:10.1016/j.ceramint.2006.08.016

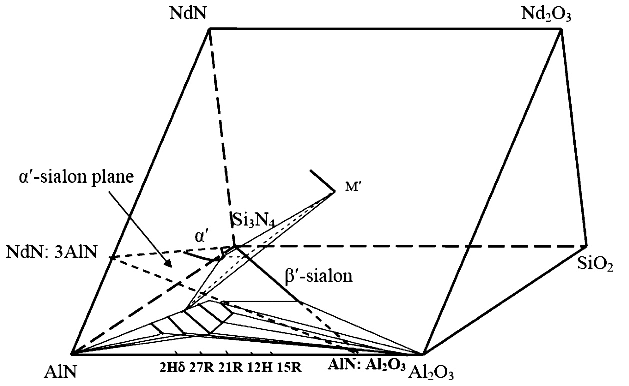

Fig. 1. Schematic illustration of the Janecke prism of Nd–Si–Al–O–N system.

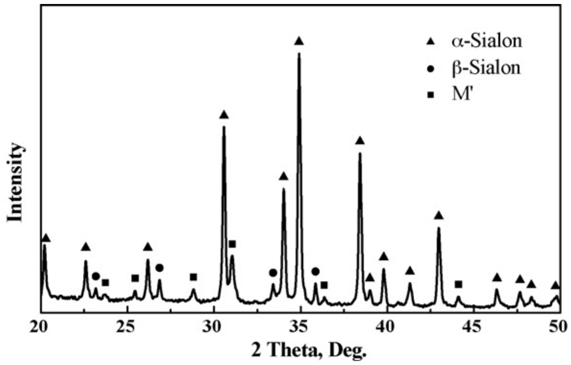

Fig. 2. XRD spectra of Nd-α-sialon ceramics after hot-pressing sintering.

paid to the microstructure development of α-sialon doped with Nd_2O_3. The phase variation process and nucleation and growth modes of different phase during sintering were also discussed.

2. Experimental procedures

The overall compositions of the investigated material were $Nd_{0.333}Si_{10}Al_2ON_{15}$, i.e., $m = n = 1$ in the general formula of α-sialon, $M_{m/3}Si_{12-(m+n)}Al_{(m+n)}O_nN_{16-n}$. The compositions lie inside the single-phase α-sialon region on the α-sialon plane (Fig. 1). An excess of 2 wt.% Nd_2O_3 was added to achieve complete densification. Starting powders used in this study are α-Si_3N_4 (E10 grade, UBE Industries Ltd., Tokyo, Japan), Al_2O_3 (grade A16SG, Alcoa, Pittsburgh, PA), AlN (grade C, H.C. Starck, Berlin, Germany), Nd_2O_3 (grade fine, H.C. Starck). When calculating the overall compositions, the contents of SiO_2 (2.38 wt.%) and Al_2O_3 (1.83 wt.%) on the surface of Si_3N_4 and AlN powders, respectively, were taken into account.

The mixed powders were ball-milled in absolute ethanol for 8 h with Si_3N_4 balls as the mixing media, and then dried at 40 °C in a rotary evaporator and sieved. Powders mixtures were hot-pressed under a uniaxial pressure of 30 MPa in a graphite resistance furnace. A two-step sintering procedure was applied, i.e. samples were first heated at a rate of 20 °C/min to 1500 °C and held there for 1 h, then heated to 1900 °C at a rate of 30 °C/min and held there again for 1 h under 0.4 MPa of nitrogen. After sintering, the samples were cooled spontaneously in the furnace.

The bulk densities of the sintered specimens were measured according to Archimedes' principle. Phase analysis was performed using X-ray diffraction (XRD). Microstructures of sintered samples on the molten NaOH etched section were observed by scanning electron microscopy (SEM). The microstructures were also characterized in detail by transmission electron microscopy (TEM) fitted with an energy dispersive X-ray spectrometer (EDS). Thin foil specimens were prepared by dimpling and subsequent ion-beam thinning.

3. Results

Full density Nd-α-sialon ceramics were obtained by the two-step hot-pressing sintering used in this study. The phase assemblages of the as-sintered Nd-α-sialon were determined by XRD, as shown in Fig. 2. It is mainly composed of α-sialon phase, with a small amount of β-sialon and secondary crystalline phase M′ ($Nd_2Si_{3-x}Al_xO_{3+x}N_{4-x}$).

Fig. 3 shows the typical microstructure of Nd-α-sialon grains. Like α-sialon doped with other rare-earth cations, Nd-α-sialon also consists of equiaxed and elongated grains with high aspect ratio.

TEM images of the sintered Nd-α-sialons, shown in Fig. 4, indicate a nearly full densified materials with the elongated α-sialon grains embedded into the fine α-sialon matrix. It is noted that in the large elongated α-sialon grain always exists core/shell structure, with some misfit dislocations at the core/shell interface. The photograph at the upper right corner is the electron diffraction pattern of the elongated grain, which reveals that the detected phase is α-sialon with hexangular structure. The zone axis is $[0\,\bar{1}\,0]$. And the core and the shell have the same structure and crystallographic orientation, as shown in Fig. 4 insert. Fig. 4(b) and (c) are EDX patterns of the core and shell of the elongated grain, respectively. It is found that compositions of the core are similar to that of the shell, and rare-earth element Nd was detected in both sites, and the concentrations of Al and O elements are high in the core. Therefore, it is reasonable to believe that this elongated α-sialon grain

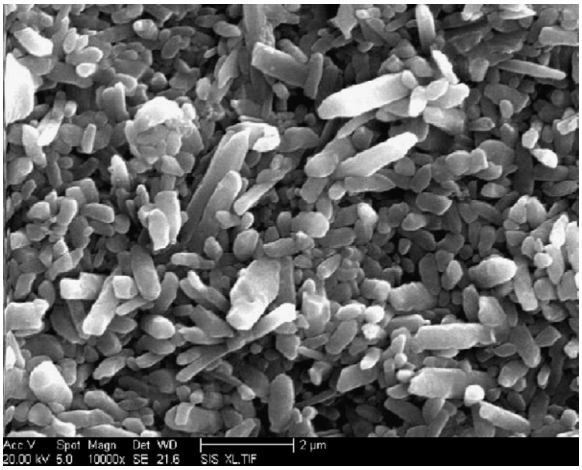

Fig. 3. SEM morphology of as-etched Nd-α-sialon ceramics.

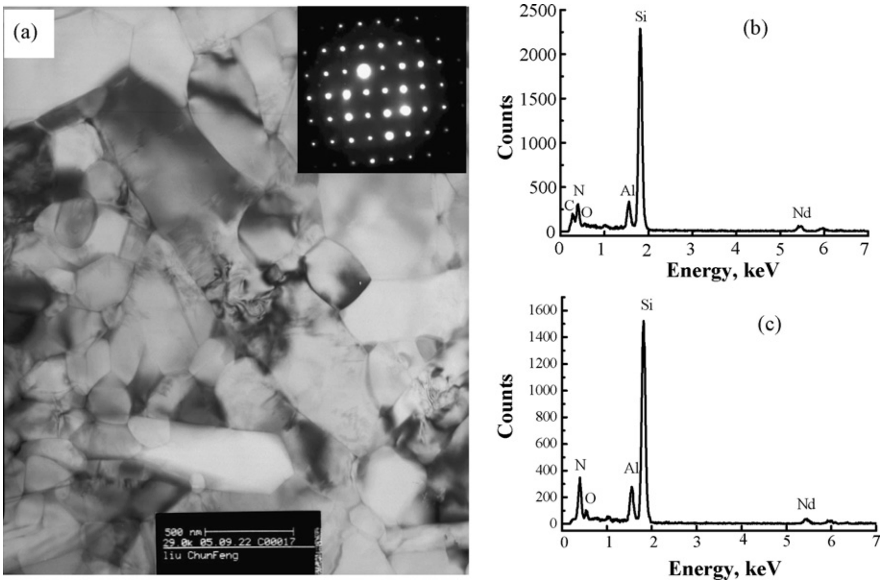

Fig. 4. TEM micrographs of as-sintered Nd-α-sialon ceramics. (a) TEM bright-field image of Nd-α-sialon, (b) EDX pattern of the core, and (c) EDX pattern of the elongated grain shell.

nucleated from the α-sialon core which formed during initial precipitation, and then grew. This nucleation and growth mode has been proposed in Ref. [24] when investigating β-sialon grains. For equiaxed α-sialon grains, few core/shell structure can be found, moreover, the compositions of the center and the edge of grains are similar. It implies that these equiaxed grains precipitated from the liquid phase and then grew.

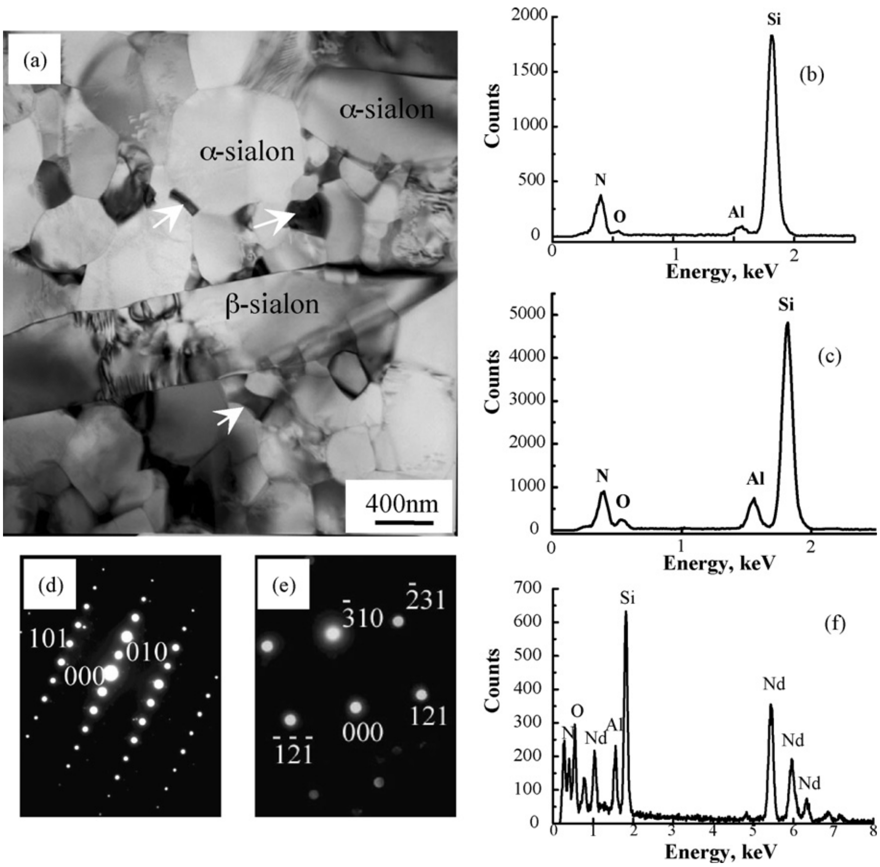

Fig. 5. TEM micrographs of β-sialon grain and intergranular phase in the Nd-α-sialon. (a) TEM bright-field image, (b) and (c) EDX patterns of the core and the shell of β-sialon, (d) and (e) SAD patterns of β-sialon and intergranular phase, and (f) EDX pattern of intergranular phase.

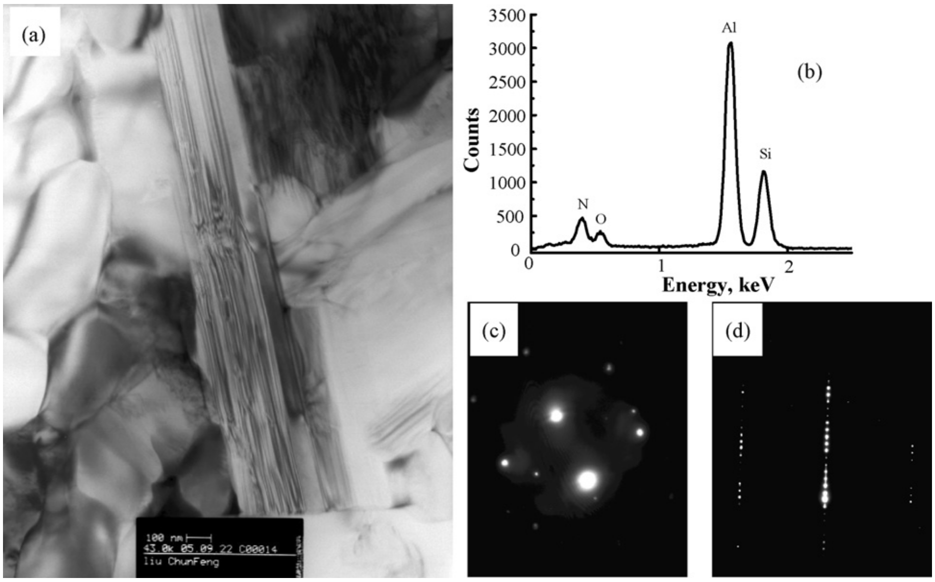

Fig. 6. TEM micrographs of 21R in the Nd-α-sialon ceramic. (a) Morphology of 21R, (b) EDX pattern of 21R, (c) and (d) SAD patterns of 21R.

The β-sialon grain with a high aspect ratio appeared in Nd-α-sialon ceramics as indicated in Fig. 5. Similar to the above α-sialon morphology, the core/shell structure is also observed in this elongated β-sialon grain. The core and shell of the grain were chosen to perform EDS analysis indicated in Fig. 5(b) and (c). The spectrum taken from the core contains Si and N, with very weak peaks of O and Al. In contrast, the pattern taken from the shell contains strong peaks of O and Al besides Si and N. Because of the small size of the core and the possible drift of the foil position during data collection, it is difficult to completely avoid the signal contribution from the adjacent grains. Moreover, maybe due to the falling off of the core during the preparing of the TEM samples, it is difficult to find an integrated core. The core, which is different in contrast from the β-sialon shell, was surrounded by some dislocations. The appeared dislocations also show evidence that there exists distortion at the interface between the core and the shell for the different composition and lattice constants. Dislocations also possibly resulted from the thermal mismatch between the core and shell during cooling. Additionally, moiré fringes were observed at such angles in the bright-field image, which implies a small rotational misfit between the core and shell. Fig. 5(d) shows the SAD pattern of the β-sialon grain. The reflection direction is $[1\,0\,\bar{1}]$. Thus, a conclusion can be drawn that the elongated grain is most likely to nucleate from Si_3N_4 particle and then grow. The mode that the elongated β-sialon grains are thought to nucleate and grow along the supersaturated β-sialon core according to Ref. [24] is contradictory to the EDS pattern of the core in this research. In this mode, the concentrations of Al and O are much higher in the core than those in the shell region.

Fig. 5 also shows the morphology and distribution of the intergranular phase (arrowed). The intergranular phases commonly distribute at the three- and four-grain junctions. Fig. 5(e) and (f) are SAD and EDX patterns of the intergranular phase, respectively. Combining both the patterns, the phase can be determined as crystallized melilite ($Nd_2Si_{3-x}Al_xO_{3+x}N_{4-x}$), abridged as M′, which is consistent with the result obtained from XRD pattern.

The existence of fiber-like phase was also observed under TEM, as represented in Fig. 6. EDX analysis (Fig. 6(b)) reveals that it contains Si, Al, O and N, moreover, the concentration of Al is much higher than Si, which is different from those in β-sialon grain. Combining the SAD patterns (Fig. 6(c) and (d)), it can be determined as 21R AlN-polytypoid phase. The composition of 21R is $6AlN{\cdot}SiO_2$. 21R AlN-polytypoid belongs to hexagonal system with rhomb-centered lattice, and the lattice parameter is $a = 3.050$ nm, $c = 56.55$ nm. Ref. [25] proposed that the fiber-like AlN-polytypoid phase can provide a valid way to reduce the amount of intergranular phase and also presents a toughening effect on the mechanical properties of the ceramics. In this work, due to the slight amount of 21R, it cannot be detected by XRD.

4. Discussion

During firing, several transformations were likely to occur as listed in the following: $\alpha\text{-}Si_3N_4 \rightarrow \alpha$-sialon, $\alpha\text{-}Si_3N_4 \rightarrow \beta$-sialon. All these transformations are known to be of a reconstructive type and usually occur through a solution-reprecipitation process in the presence of a liquid phase.

Since the surfaces of nitride particles are always covered with an oxygen-rich layer, an oxide subsystem SiO_2–Al_2O_3–Nd_2O_3 is supposed to be presented in the mixture. As the temperature increases, the oxides react to form a eutectic liquid phase [26]. According to acid-alkali theory proposed by Menon and Chen [27,28], large rare-earth is more basic, and hence favors the reaction with a more acidic Si–N in preference to a less acidic Al–N. This trend has been seen in various wetting reactions and intermediate phase reactions in complex SiAlON system [27]. That is, Si_3N_4 powders can solute into the liquid quickly. That means much α-sialon should be formed. But owing to the large size of Nd^{3+} (1.00 Å), in particular, in the early stage of sintering, it is difficult to enter and exist stably in the lattice interstice of Si_3N_4 for Nd cations. Melilite (M′) has been observed more stable in materials with large modifying cations, like Nd, Gd and Dy, which have smaller single regions for the α-sialon [29]. Thus, at lower temperature, the instability of Nd-α-sialon results in the precipitation of more stable β-sialon and Nd-M′ phases. Ref. [14] also proposes that the stability of α-sialon decreases at lower temperatures and especially with larger cations, and α-sialon region becomes smaller than that at higher temperature. This means that at lower temperature stage, the adopted compositions in this study most likely lies outside the single-phase α-sialon region, and belong to the α + β-sialon region in the α-sialon plane, as shown in Fig. 1. As the temperature rising, the single-phase α-sialon region becomes larger, the compositions lie inside. Besides, the vibration of Si_3N_4 lattice aggravates, and the interstice turns larger. Nd cations can enter the interstice easily and form relatively stable Nd-α-sialon phase. At the meantime, as-formed β-sialon and Nd-M′ phases resolve again, which provides raw materials for precipitation of α-sialon, nevertheless a small amount of β-sialon phases still contaminate and coexist with α-sialon phase. And correspondingly, much cations have been remained at the boundary. When cooled, the transient liquid phase containing much Nd cations crystallized to form intergranular phase. Because the α′(α-sialon)-β′(β-sialon)-21R triangle is located closer to the NdN–AlN–Si_3N_4 plane in the Nd system than the α′-β′-12H triangle in the Yb system, this would result in a higher amount of intergranular phase in the case of Nd than in Yb [29]. Our research results are consistent with the reported results [30]. In the process of sintering, AlN-polytypoid as AlN solid solution is formed via replacing Al–N bond by Si–O bond. And the final type is 21R in Nd system, which coincides with others' research [29]. The compatibility tetrahedral α′(α-sialon)-β′(β-sialon)-21R-M′ has been proved to exist in the Nd–Si–Al–O–N system [17], as presented in the Janecke prism (Fig. 1).

Although the lattice misfit is relatively large between α-Si_3N_4 and β-sialon versus that between β-Si_3N_4 and β-sialon [31,32], α-Si_3N_4 particles do act as nuclei for β-sialon in this research. With the solution of α-Si_3N_4 particles, more stable β-sialon and intermediate phases begin to precipitate. The β-sialon grows via precipitation on insoluted α-Si_3N_4 particle, thus a structure of core and shell is found in the material. In Nd–SiAlON system, α-Si_3N_4 particles solute quickly and correspondingly, α-sialon can nucleates early and the amount of nuclei is high. However, due to the instability of α-sialon and the competition of intermediate phases with α-sialon for the raw materials, α-sialon grains grow slowly. At the high temperatures, with the intermediate phase soluting, α-sialon phases grow gradually, and some grow along the initial α-sialon grains produced at lower temperature to form the anisotropic elongated grains with core/shell structure.

5. Conclusions

Fully density Nd-α-sialon was obtained by a two-step hot-pressing sintering. The ceramic mainly consists of elongated α-sialon grains with high aspect ratio embedded in finer equiaxed α-sialon grains. Also there exist a small amount of β-sialon and intergranular phase M′ as well as slight amount of 21R AlN-polytypoid. Equiaxed α-sialon grains precipitate from liquid directly, but the elongated ones with core/shell structure grow with the primarily precipitated α-sialon as seeds. Differently, β-sialon nucleates and grows from Si_3N_4 core. It is difficult for larger Nd cations to enter Si_3N_4 structure, which leads to the remnant of M′ phases at the boundary.

References

[1] T. Ekström, M. Nygren, Sialon ceramics, J. Am. Ceram. Soc. 75 (2) (1992) 259–276.

[2] G.Z. Gao, R. Metselaar, α′-Sialon ceramics: a review, Chem. Mater. 3 (2) (1991) 242–252.

[3] I.-W. Chen, A. Rosenflanz, A tough SiAlON ceramic based on α-Si_3N_4 with a whisker-like microstructure, Nature (London) 389 (1997) 701–704.

[4] Z.J. Shen, H. Peng, P. Pettersson, M. Nygren, Self-reinforced α-sialon ceramics with improved damage tolerance developed by a new processing strategy, J. Am. Ceram. Soc. 85 (11) (2002) 2876–2878.

[5] H. Peng, Z.J. Shen, M. Nygren, The formation of in-situ reinforced microstructure in α-sialon ceramics. II. In the presence of a liquid phase, J. Mater. Res. 17 (5) (2002) 1136–1142.

[6] I.H. Shin, D.J. Kim, Growth of elongated grains in α-sialon ceramics, Mater. Lett. 47 (2001) 329–333.

[7] C.A. Wood, H. Zhao, Y.B. Cheng, Microstructure development of calcium α-sialon ceramics with elongated grains, J. Am. Ceram. Soc. 82 (2) (1999) 421–428.

[8] Z.B. Yu, D.P. Thompson, A.R. Bhatti, In situ growth of elongated α-sialon grains in Li-α-sialon ceramics, J. Eur. Ceram. Soc. 20 (2000) 1987–1995.

[9] P.L. Wang, W.Y. Sun, T.S. Yen, Sintering and formation behavior of R-α-sialons (R = Nd, Sm, Gd, Dy, Er and Yb), Eur. J. Solid State Inorg. Chem. 31 (1994) 93–104.

[10] H. Peng, Z.J. Shen, M. Nygren, Reaction sequences occurring in dense Li-doped sialon ceramics: influence of temperature and holding time, J. Mater. Chem. 13 (2003) 2285–2289.

[11] F. Ye, M.J. Hoffmann, S. Holzer, Y. Zhou, M. Iwasa, Effect of the amount of additives and post-heat treatment on the microstructure and mechanical properties of yttrium-α-sialon ceramics, J. Am. Ceram. Soc. 86 (12) (2003) 2136–2142.

[12] J.S. Kim, A. Rosenflanz, I.-W. Chen, Microstructure control of *in-situ*-toughened α-SiAlON ceramics, J. Am. Ceram. Soc. 83 (7) (2000) 1819–1821.

[13] S. Bandyopadhyay, M.J. Hoffmann, G. Petzow, Effect of different rare earth cations on the densification behaviour of oxygen rich α-SiAlON composition, Ceram. Int. 25 (1999) 207–213.

[14] A. Rosenflanz, I.-W. Chen, Phase relationships and stability of α′-SiAlON, J. Am. Ceram. Soc. 82 (4) (1999) 1025–1036.

[15] Z.K. Huang, I.-W. Chen, Rare-earth melilite solid solution and its phase relations with neighboring phases, J. Am. Ceram. Soc. 79 (8) (1996) 2091–2097.

[16] W.Y. Sun, H.Y. Tu, P.L. Wang, D.S. Yan, Nitrogen-rich liquid phase regions in the Ln–Si–Al–O–N (Ln = Nd, Sm, Gd, Dy, Er and Yb) system, J. Eur. Ceram. Soc. 17 (1997) 789–796.

[17] W.Y. Sun, D.S. Yan, L. Gao, H. Mandal, K. Liddell, D.P. Thompson, Subsolidus phase relationships in the systems Ln_2O_3–Si_3N_4–AlN–Al_2O_3 (Ln = Nd, Sm), J. Eur. Ceram. Soc. 15 (1995) 349–355.

[18] L.-O. Nordberg, M. Nygren, P.-O. Käll, Z.J. Shen, Stability and oxidation properties of RE-α-sialon ceramics (RE = Y, Nd, Sm, Yb), J. Am. Ceram. Soc. 81 (6) (1998) 1461–1470.

[19] H. Mandal, N. Camuscu, D.P. Thompson, Comparison of the effectiveness of rare-earth sintering additives on the high-temperature stability of α-sialon ceramics, J. Mater. Sci. 30 (1995) 5901–5909.

[20] J. Yu, H. Du, R. Shuba, I.-W. Chen, Dopant-dependent oxidation behavior of α-SiAlON ceramics, J. Mater. Sci. 39 (2004) 4855–4860.

[21] M. Mitomo, A. Ishida, Stability of α-sialon in low temperature annealing, J. Eur. Ceram. Soc. 19 (1999) 7–15.

[22] S.L. Hwang, I.-W. Chen, Nucleation and growth of α'-SiAlON on α-Si_3N_4, J. Am. Ceram. Soc. 77 (7) (1994) 1711–1718.

[23] F.F. Xu, S.L. Wen, L.O. Nordberg, T. Ekstrom, Nucleation and growth of the elongated α'-SiAlON, J. Eur. Ceram. Soc. 17 (1997) 1631–1638.

[24] S.L. Hwang, I.-W. Chen, Nucleation and growth of β'-SiAlON, J. Am. Ceram. Soc. 77 (7) (1994) 1719–1728.

[25] P.L. Wang, C. Zhang, W.Y. Sun, D.S. Yan, Formation behavior of multication α-sialons containing calcium and magnesium, Mater. Lett. 38 (1999) 178–185.

[26] T. Ekström, Preparation and properties of α-Si–Al–O–N Ceramics, J. Hard Mater. 3 (2) (1992) 109–118.

[27] M. Menon, I.-W. Chen, Reaction densification of α-sialon. I. Wetting behavior and acid–base reactions, J. Am. Ceram. Soc. 78 (3) (1995) 545–554.

[28] M. Menon, I.-W. Chen, Rection densification of α-sialon. II. Densification behavior, J. Am. Ceram. Soc. 78 (3) (1995) 554–559.

[29] A. Rosenflanz, I.-W. Chen, Kinetics of phase transformation in SiAlON ceramics. I. Effect of cation size, composition and temperature, J. Eur. Ceram. Soc. 19 (1999) 2325–2335.

[30] C.F. Liu, F. Ye, Y. Zhou, Q.C. Meng, Y.L. Wang, Microstructure of different rare-earth-doped α-sialon ceramics, Key Eng. Mater., in press.

[31] W.Y. Sun, T.Y. Tien, T.S. Yan, Solubility limits of α'-SiAlON solid solutions in the system Si, Al, Y/N, O, J. Am. Ceram. Soc. 74 (10) (1991) 2547–2550.

[32] M. Havier, O. Johannesen, Unit-cell dimension of β'-SiAlON, Adv. Ceram. Mater. 3 (4) (1988) 405–407.